Theor Chem Acc (2012) 131:1125
DOI 10.1007/s00214-012-1125-y

REGULAR ARTICLE

Computational methodology for chirality determination in the Soai reaction by crystals: γ-glycine

Damien J. Carter · Bart Kahr · Andrew L. Rohl

Received: 17 November 2011 / Accepted: 21 December 2011 / Published online: 9 February 2012

Abstract The autocatalytic Soai reaction gives abundant evidence of the enantioselective adsorption of organic compounds on a variety of crystals. Computational modelling can provide insight into mechanisms of enantioselectivity. Here, we use a combination of simulated annealing, forcefield, and quantum mechanical methods to examine interactions of pyrimidyl-5-carbaldehyde and 2-methylpyrimidyl-5-carbaldehyde with surfaces of γ-glycine. Using binding energy results, we predict the exposure of the prostereogenic *S* face of pyrimidyl-5-carbaldehyde (~65%) and 2-methylpyrimidyl-5-carbaldehyde (>90%) on the (1 $\bar{1}$ 0) and ($\bar{1}$ 1 0) surfaces. The aim is to develop a robust computational methodology that can be applied to understanding crystal-biased asymmetric synthesis.

Keywords Molecular modelling · Soai reaction · Crystal surfaces · Enantioselectivity

1 Introduction

Reactions with nonlinear kinetics can have surprising stereochemical consequences [1]. Nowhere is this more dramatic than in Soai's reaction [2–6] in which an organo-zinc catalyst with the slightest [7–10] enantiomeric excess (ee) is sufficient to generate >95% ee of alkylated achiral aldehydes. The relevance of stochastic fluctuations [11, 12] followed by asymmetric autocatalysis may well be responsible for chirobiogenesis [13–15].

The Soai reaction can be heterogeneously catalysed by the surfaces chiral crystals such as sodium chlorate [16], sodium bromate, quartz [17, 18], benzyl [19], hippuric acid [20], cytosine [21], 1,1′-binaphthyl [22], and a variety of organic co-crystals [23]. Soai reactions with enantiomorphous crystals are deterministic; dextrorotatory quartz (SiO_2) or sodium chlorate ($NaClO_3$) produce alcohols with the *S*-configuration from **1** (2-(3,3-dimethylbut-1-yn-1-yl)pyrimidine-5-carbaldehyde), whereas levorotatory quartz or $NaClO_3$ produce alcohols with the *R*-configuration (see Fig. 1). The autocatalytic Soai reaction gives abundant evidence of enantioselective adsorption of organic compounds to a variety of crystals but adsorbate–crystal interactions have yet to be described. Here, we examine to what extent computational crystallography methodologies can address some of these mechanisms. DFT calculations have been used to study the intermediates in the Soai reaction, but have not been used to assay the role of crystals [24–27].

Under ambient conditions, three polymorphs of glycine ($\alpha - P2_1/n$, $\beta - P2_1$, and $\gamma - P3_{1(2)}$) have been described [28]. In the γ-polymorph, chains of zwitterions form three distinct helices that are linked to one another [29]. The crystal structure of γ-glycine is illustrated in Fig. 2. The γ-form is the most thermodynamically stable glycine; however, it is often overwhelmed in crystallisation by the kinetically favoured α-form. Nevertheless, very slow crystallisation from neutral solutions [30], irradiation of the crystallisation solution with plane-polarised laser light [31], and the addition of additives [32, 33] have been reported to yield γ-glycine.

D. J. Carter (✉) · A. L. Rohl
Department of Chemistry, Nanochemistry Research Institute, Curtin University, Perth, WA, Australia
e-mail: d.carter@curtin.edu.au

D. J. Carter · A. L. Rohl
iVEC, Technology Park, Kensington, WA, Australia

B. Kahr
Department of Chemistry, New York University, New York, NY, USA

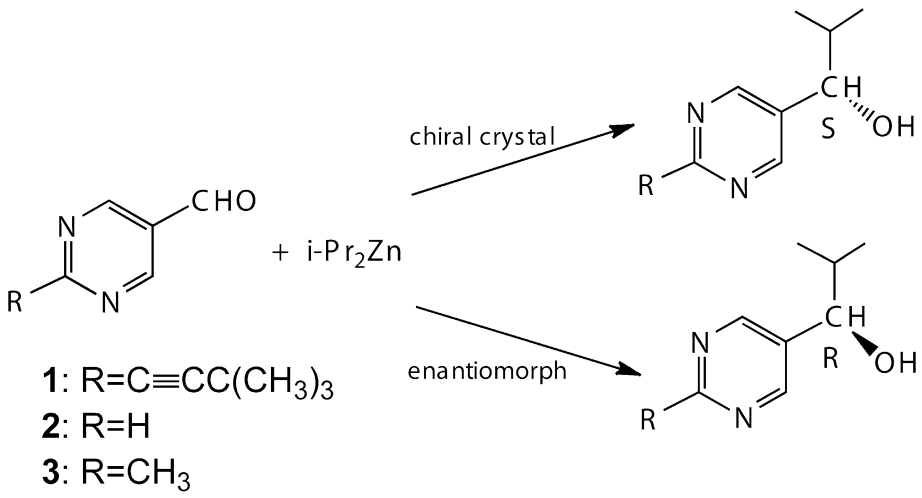

Fig. 1 Absolute structures of chiral crystal additives establish configurations. For **1**, *d*-quartz gives *S* alkanol in 97% ee, and *l*-quartz gives *R* alkanol. *d*-$NaClO_3$ gives *S* (98% ee); *l*-$NaClO_3$ gives *R* (98% ee) [2]

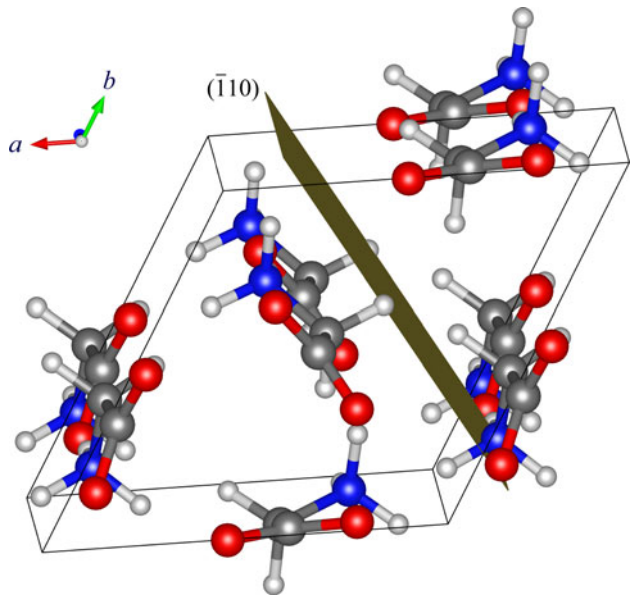

Fig. 2 The crystal structure of γ-glycine with the $\{\bar{1}\ 1\ 0\}$ cleavage plane *highlighted*. Carbon, hydrogen, nitrogen, and oxygen atoms are shown as *dark grey-*, *light grey-*, *blue-*, and *red-coloured spheres*, respectively

γ-Glycine does indeed catalyse the Soai reaction [34]. Glycine, the simplest amino acid, draws the Soai reaction closer to realistic prebiotic chemistry. However, because the absolute structure of glycine crystals has yet to be assigned, we do not know which enantiomorphous crystal catalyses the formation of which enantiomer during the alkylation reaction. In this case, computations may serve as a prediction. The γ-form of glycine shows hexagonal prism ($\{0\ 1\ 0\}$, $\{\bar{1}\ 1\ 0\}$) and pyramidal faces ($\{0\ 1\ 1\}$, $\{\bar{1}\ 1\ 1\}$) varying in proportion according to the conditions of growth. $(0\ 0\ \bar{1})$ is also present but poorly developed [15]. The crystals show a bipyramidal habit under some conditions via twinning across the $(0\ 0\ \bar{1})$. Whatever the habit, the crystals tend to show weak cleavage parallel to the *c* axis [29]. This observation, and the results of computations below, leads us to presume that the predominant $\{hkl\}$ surfaces exposed on cleavage are $\{\bar{1}\ 1\ 0\}$ and $\{1\ \bar{1}\ 0\}$ (highlighted in Fig. 2).

A prerequisite of any computational investigation of the role of crystals in the Soai reaction is an accounting of the mechanism of autocatalysis and amplification as it is presently understood. Blackmond and coworkers [35–40] established through kinetic measurements the order of the reactants and intermediates. Brown and coworkers [41–44] established by NMR and computation the structures of some predominant solution aggregates. These facts were combined in a model of a catalytic cycle [45] that neatly accounts for both autocatalysis and chirality amplification. However, the mechanism does not account for the deterministic influence of chiral additives in solution or the action of chiral crystal surfaces. Key steps in the afore-cited Schiaffino/Ercolani mechanism involve the formation of an aggregate of four homochiral zinc complexes that disassociates into two pairs one of which reenters the cycle by capturing and then reducing two additional aldehyde reactants. Surely, this is not the last word defining the Soai mechanism, but our understanding has been advanced considerably by the impressive, aforementioned investigations.

Where in this cycle does a crystal intercede heterogeneously? Crystals could indeed interact enantioselectively with any of the solution intermediates that have been proposed. We do not know which? Therefore, the simplest possibility to investigate computationally is the adsorption of Soai pyrimidinecarbaldehydes. The achiral aldehydes bind to chiral surfaces so as to preferentially expose a prostereogenic face to the solution containing the alkylation reagent. Here, we propose to address this question using a combination of forcefield and quantum mechanical

computations. We have recently demonstrated the combination of simulated annealing with forcefield calculations for predicting enantioselective binding of tartaric acid to chiral surfaces of resorcinol [46].

Molecular mechanics (MM) calculations and density functional theory (DFT) calculations were used to examine the interactions of pyrimidine-5-carbaldehyde (**2**) and 2-methylpyrimidine-5-carbaldehyde (**3**) with the most stable surfaces of γ-glycine. Molecular mechanics calculations, in particular simulated annealing methods, sampled a large number of potential orientations of **2** and **3** with the most stable orientations subsequently used as starting configurations for the more accurate but computationally demanding DFT calculations.

2 Methodology

Molecular mechanics calculations were carried out using the Materials Studio software package [47]. Electrostatic interactions were computed with an Ewald summation to an accuracy of 1×10^{-5} kcal/mol, and atomic charges were assigned by the forcefield. van der Waals interactions were embodied in atom-based summation with a cutoff of 18.5 Å. Density functional theory calculations were carried out using the SIESTA code [48] with the generalised gradient approximation of Perdew et al. [49]. Atoms were described by norm-conserving pseudopotentials with a double zeta basis-set including polarisation functions. The localised basis-set in SIESTA consists of numerical atomic orbitals radially confined to an extent that induces an energy shift in each orbital of 0.01 Ry. Hartree and exchange–correlation energies were evaluated on a uniform real space grid of points with a defined maximum kinetic energy of 150 Ry.

Structural optimisation of γ-glycine was performed with CVFF [50] and COMPASS [51, 52] forcefields within the Materials Studio Forcite module as was a morphology prediction with fixed surfaces. The $(\bar{1}\ 1\ 0)$ and $(1\ \bar{1}\ 0)$ surfaces were the most stable, based upon the attachment energies. The $(\bar{1}\ 1\ 0)$ and $(1\ \bar{1}\ 0)$ surfaces have different chemical structures for the acentric γ-glycine, but more importantly, when stable surface terminations for the $(\bar{1}\ 1\ 0)$ surface are cleaved from bulk γ-glycine, the opposite surface is always the $(1\ \bar{1}\ 0)$, and vice versa. All MM and DFT calculations have been performed using 3D periodic simulation cells, where $(\bar{1}\ 1\ 0)$ and $(1\ \bar{1}\ 0)$ surfaces are separated by a vacuum region. The $(\bar{1}\ 1\ 0)/(1\ \bar{1}\ 0)$ surfaces can be cleaved in three chemically unique ways at 0.0, 0.16, and 0.49. The most stable termination was determined by calculating the surface energy, as given by the equation:

$$E_{\text{surf}} = (E_{\text{slab}} - E_{\text{equiv bulk}})/2A$$

where E_{surf} is the surface energy, E_{slab} is the energy of the surface slab with a vacuum gap, $E_{\text{equiv bulk}}$ is the energy of the surface slab with no vacuum gap, and A is the surface area. E_{surf} is divided by two because each slab has two surfaces and thus the surface energy is actually an average of the $(\bar{1}\ 1\ 0)$ and $(1\ \bar{1}\ 0)$ surface energies at the opposite sides of the slab.

Docking calculations were carried out using a 6-repeat layer supercell, with a 20-Å vacuum gap in the direction normal to the surface to ensure periodic images did not interact. Simulated annealing calculations were carried out using the Adsorption Locator module in Materials Studio, keeping the surfaces fixed but allowing **2** and **3** complete freedom of motion. Each simulated annealing calculation involved 1,000 loading steps, 1,000 heating cycles per run (with starting and final temperatures of 500 and 300 K, respectively), 100 steps per run, and the geometry was optimised at the end of each run. In all cases, the entire simulated annealing run was repeated up to six times, using both the CVFF and COMPASS forcefields. The fact that the most stable orientations appeared in numerous different runs gave us confidence that we had sufficiently sampled the entire configurational space.

For DFT calculations, a similar procedure to the molecular mechanics calculations was followed, fully optimising the bulk structure and then the three possible $(\bar{1}\ 1\ 0)$ and $(1\ \bar{1}\ 0)$ surface cuts (again calculating the surface energy to see which termination was most stable). For docking and surface calculations, we used an 8-repeat layer supercell fully relaxing all atoms, with a 40-Å vacuum gap to ensure periodic images did not interact. In total, nine stable structures of each docking molecule were chosen from the simulated annealing calculations, as starting structures for DFT docking calculations. To determine which configuration of **2** and **3** was most stable on each surface, the binding energy (E_{b}) was calculated using the equation:

$$E_{\text{b}} = E_{\text{dock}} - (E_{\text{slab}} + E_{\text{mol}})$$

where E_{dock} is the total energy of surface with the adsorbate molecule contained within it, E_{slab} is the total energy of the relaxed surface slab, and E_{mol} is the energy of an isolated, relaxed adsorbate molecule.

3 Results

We first optimised bulk γ-glycine using molecular mechanics. The lattice parameters from CVFF and COMPASS were $a = 6.963$, $c = 5.560$ Å, and $a = 7.243$, $c = 5.086$ Å, respectively, compared to the experimental lattice parameters of $a = 7.046(3)$ Å and $c = 5.491(2)$ Å

[53]. Somewhat surprisingly, the older protein-optimised CVFF forcefield appears to perform better than the solid-state-optimised COMPASS forcefield, so both were used in all subsequent calculations for comparison. The DFT-optimised γ-glycine cell parameters were $a = 7.056$ Å and $c = 5.463$ Å, and as expected differ from experiment by approximately 1%.

The energies of the unrelaxed surfaces were calculated using molecular mechanics. For the three possible ($\bar{1}$ 1 0)/(1 $\bar{1}$ 0) surface terminations, the surface energies were 0.13, 0.19, and 0.18 J/m^2 using COMPASS and 0.23, 0.29, and 0.27 J/m^2 using CVFF (the surface cuts were 0.0, 0.16, and 0.49, respectively). When we attempted to relax the stable surfaces, we found that both the CVFF and COMPASS failed to preserve the zwitterionic state of the γ-glycine molecules. For this reason, we fixed the surfaces in simulated annealing calculations but fully relaxed **2** and **3**. In DFT calculations, all surfaces were fully relaxed, and in contrast to the forcefield results, the γ-glycine surfaces displayed zwitterionic molecules. The DFT-relaxed surface energies were 0.24, 0.29, and 0.34 J/m^2 for the three surface cuts (0.0, 0.16, and 0.49, respectively). In all cases, the surface cut of 0.0 was the most stable (lowest surface energy), so this surface termination was used for all subsequent docking MM and DFT docking calculations.

From the results of simulated annealing calculations, the nine most stable orientations of **2** and **3** on the ($\bar{1}$ 1 0) and (1 $\bar{1}$ 0) surfaces were chosen. In general, the most stable orientations of **2** and **3** on both surfaces show that the long axis of the docking molecule is essentially parallel to the surface and lies along one of the surface vectors, with the pyrimidine slightly tilted towards the surface to maximise the interactions (detailed later) with the surface below. These most stable orientations were then used as starting structures for DFT docking studies. The binding energies for the three most stable orientations of **2** and **3** docked onto the ($\bar{1}$ 1 0) and (1 $\bar{1}$ 0) surfaces calculated using DFT are reported in Table 1 and are illustrated in Figs. 3 and 4, respectively.

Overall, the most stable configurations of **2** and **3** on each of the surfaces are quite similar. On the ($\bar{1}$ 1 0) surface, both docking molecules have their pyrimidine ring tilted towards the surface at approximately a 45 degree angle, with the oxygen atom of the aldehyde group pointing towards the surface. On the (1 $\bar{1}$ 0) surface, both docking molecules have the pyrimidine ring almost flat on the surface, with the oxygen atom of the aldehyde group on the opposite side to that on the ($\bar{1}$ 1 0) surface. As mentioned previously, because γ-glycine is acentric, the structures of the ($\bar{1}$ 1 0) and (1 $\bar{1}$ 0) surfaces are quite different. In Figs. 3 and 4, **2** and **3** appear to fit quite nicely within the higher ridges on the (1 $\bar{1}$ 0) surface and thus lie quite flat on the surface. On the ($\bar{1}$ 1 0) surface, there is not enough room to accommodate the adsorbate that therefore tilts.

Table 1 Binding energies for the three most favourable orientations of **2** and **3** docked on the ($\bar{1}$ 1 0) and (1 $\bar{1}$ 0) surfaces of γ-glycine

	Binding energy (kJ/mol)	
	2	**3**
($\bar{1}$ 1 0)		
Orientation 1	−164.5	−177.0
Orientation 2	−155.8	−170.8
Orientation 3	−155.7	−165.1
(1 $\bar{1}$ 0)		
Orientation 1	−165.8	−183.7
Orientation 2	−163.0	−179.5
Orientation 3	−160.2	−170.6

To investigate the most stable orientations in more detail, we have examined the presence of hydrogen bonds and π-interactions between the pyrimidine ring and the γ-glycine surface. Desiraju and Steiner [54] suggest that strong hydrogen bonds, such as O–H···O=C and N–H···O=C, have H···A separations of approximately 1.5–2.2 Å, and weak hydrogen bonds such as C–H···O have H···A separations of approximately 2.0–3.0 Å. The most stable configuration of **2** on the ($\bar{1}$ 1 0) surface has one strong hydrogen bond and five weak hydrogen bonds, while on the (1 $\bar{1}$ 0) surface, the most stable configuration has one strong and eight weak hydrogen bonds (illustrated in Fig. 3). The most stable configuration of **3** on the ($\bar{1}$ 1 0) surface has one strong and eight weak hydrogen bonds. On the (1 $\bar{1}$ 0) surface, the most stable configuration of **3** has one strong and ten weak hydrogen bonds (illustrated in Fig. 4).

For both **2** and **3** docking molecules, there are more weak hydrogen bonds to the ($\bar{1}$ 1 0) surface than the (1 $\bar{1}$ 0) surface. The binding energies in Table 1 show the (1 $\bar{1}$ 0) surface is the preferred surface (more negative) for docking **2** and **3**, and the extra hydrogen bonding may explain why this is so. We also examined separation distances between the centroid of the pyrimidine rings of the docking molecules and neighbouring atoms on the glycine surfaces, and for each docking molecule on both the ($\bar{1}$ 1 0) and (1 $\bar{1}$ 0) surfaces, we find there are three pyrimidine···H separation distances of 3.2–3.6 Å. There appears to be no significant difference between π-interactions of the most stable configurations of the docking molecules on either surface. The most stable docking configurations (Figs. 3, 4) of the **2** and **3** molecules on both the ($\bar{1}$ 1 0) and (1 $\bar{1}$ 0) surfaces are very similar. The angle of tilt of the pyrimidine ring and the location of the aldehyde oxygen atom are very close. The

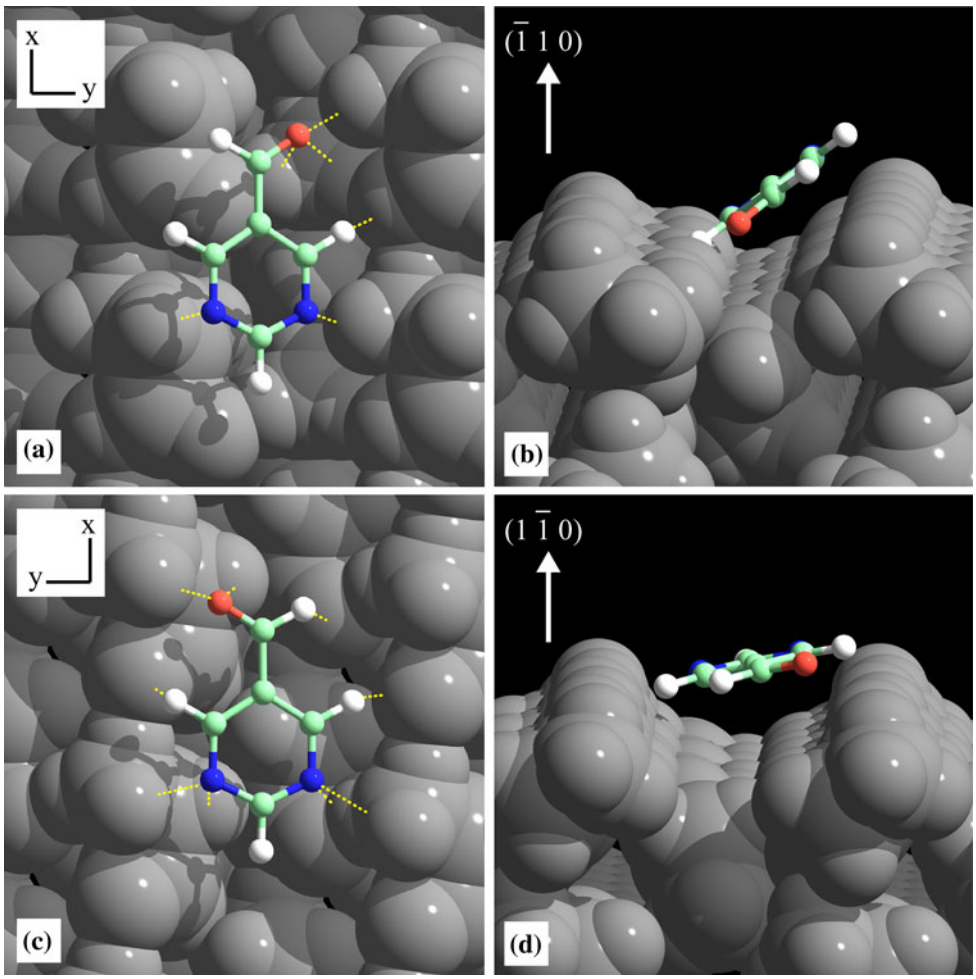

Fig. 3 The most stable orientation of **2** on the ($\bar{1}$ 1 0) surface of γ-glycine viewed from **a** above and **b** the side. The most stable orientation of **2** on the (1 $\bar{1}$ 0) surface of γ-glycine viewed from **c** above and **d** the side. In parts **a** and **c**, the *dashed lines* indicate the location of hydrogen bonds

presence of the methyl group on the pyrimidine ring appears to have little effect on the orientations of the most stable configurations of the docking molecules.

Interestingly, the most stable orientations of pyrimidylaldehyde and 2-methylpyrimidylaldehyde calculated via quantum mechanics, where the surface and molecule were relaxed, compare closely to the most stable orientations from simulated annealing calculations. In particular, using the COMPASS forcefield, the most stable orientations are almost identical. For the CVFF forcefield, we did observe some small differences between the most stable orientations; however, considering the surface was fixed in the calculations and there is no account of electronic structure in these calculations, forcefields give remarkably good results. The fact that the simulated annealing method (using both forcefields) predicted the stable structures later confirmed using DFT calculations gives us further confidence that we had sufficiently sampled the configurational space of **2** and **3** using simulated annealing calculations.

In the Ercolani–Schiaffino cycle, there are six aromatic intermediates, each one of which can enantioselectively interact with crystalline surfaces. However, before taking up these complex heterogeneous processes, we must first recognise that the Ercolani–Schiaffino mechanism requires an enantiomeric excess of alcohol. This excess can naturally form stochastically in any given reaction mixture, but a reliance on chance cannot explain the crystallographic data; *d*-$NaClO_3$ always gives *S* alcohol, for example (Fig. 1).

Using the binding energies for the most stable docking configurations in Table 1, the energy differences can be used to calculate a Boltzmann distribution. In this way, it is possible to predict a population or fraction of docking molecules that will belong to a particular adsorbate configuration. A Boltzmann distribution at 298 K was calculated for each adsorbate molecule by combining the results for docking on the ($\bar{1}$ 1 0) and (1 $\bar{1}$ 0) surfaces with the configurations designated as either left- or right-handed based on the orientations of the aldehyde group. Despite the fact that the most stable configuration on both surfaces exposed the pro-*S* face of **2** and the pro-*R* face of **3**, the Boltzmann-weighted predictions lead to the exposure of the same stereogenic face for both enantiomers. For **2,** this

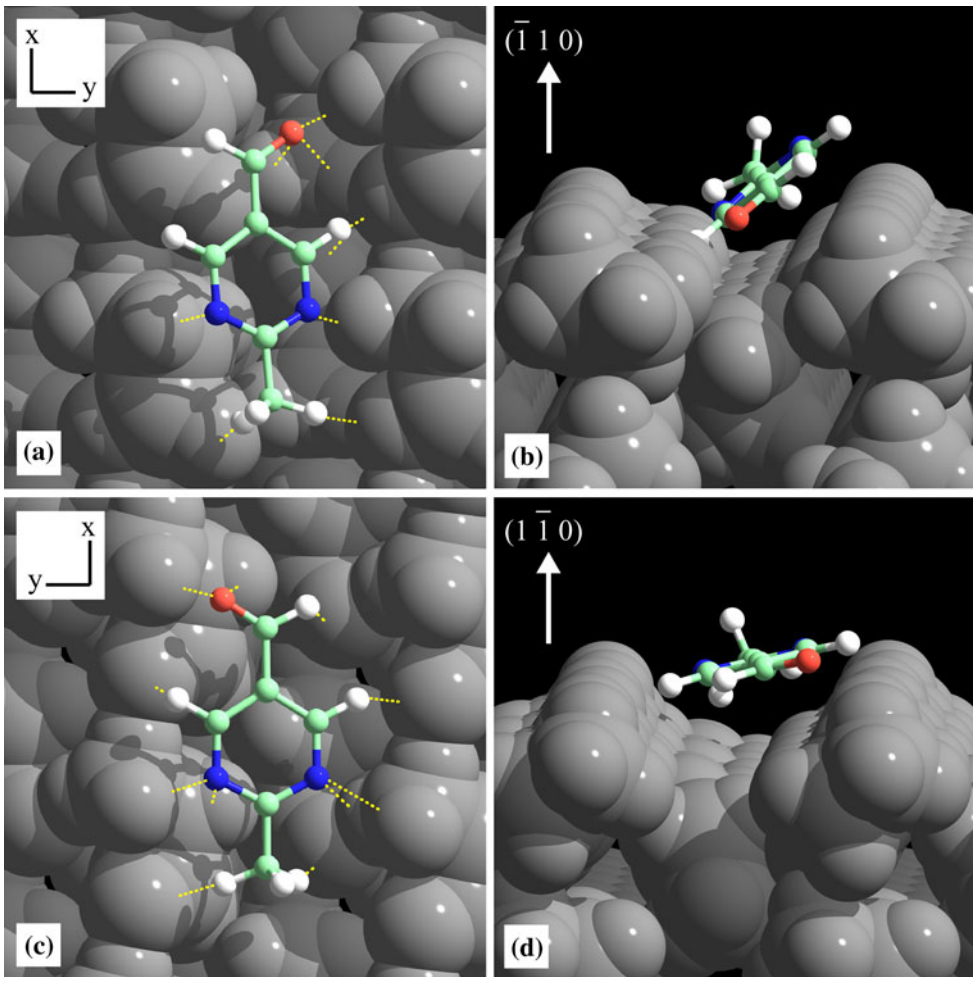

Fig. 4 The most stable orientation of **3** on the ($\bar{1}$ 1 0) surface of γ-glycine viewed from **a** above and **b** the side. The most stable orientation of **3** on the (1 $\bar{1}$ 0) surface of γ-glycine viewed from **c** above and **d** the side. In parts **a** and **c**, the *dashed lines* indicate the location of hydrogen bonds

results in 65% pro-*S* face exposed and 35% pro-*R* face exposed, while for **3**, this results in 94% pro-*S* enantiomer and 6% pro-*R* enantiomer. The Boltzmann distribution for both **2** and **3** suggests there is a weak preference for docking with pro-*S* aldehyde faces exposed, with a more decisive discrimination on ($\bar{1}$ 1 0) surfaces. The addition of the methyl group in **3** makes this preference stronger. Overall, these studies predict that **2** and **3** preferentially bind to the (1 $\bar{1}$ 0) face of γ-glycine, leading to the *S* alcohol enantiomer if the alkylating reagent is delivered from the solution to the aldehyde bound on the crystal. However, there is no experimental evidence for this step in the Soai reaction.

Experimentally, any evaluation of the role of γ-glycine in the catalysis of the Soai reaction necessitates knowledge of the absolute structure of the individual crushed γ-glycine crystals used to initiate the chiral amplification. The first determination of absolute crystallographic structure was made of sodium rubidium (+)-tartrate tetrahydrate by Bijvoet et al. [55]. The so-called Bijvoet method relies on the effects of resonant scattering from heavy atoms on diffraction intensities [56] and thus is difficult to apply to structures containing only C, H, N, and O [57]. In such cases, the direct determination of phases by multiple-beam X-ray diffraction [58] has been successful [59, 60]. However, this technique requires highly collimated radiation from a synchrotron source and the experience at establishing and interpreting interference from three beams. An independent and wholly chemical method for establishing absolute structure relies on interpreting the morphology changes induced in growing crystals by so-called tailor-made additives [61]. However, this method is predicated on an intuitive understanding of the intermolecular interactions at surfaces, and responsive morphologies. To date, we have been unable to determine the absolute structure of γ-glycine by any method but are continuing our efforts in the hope of verifying the theoretical predictions.

4 Conclusions

Molecular modelling studies of **2** and **3** interactions with (1 $\bar{1}$ 0) and ($\bar{1}$ 1 0) surfaces of γ-glycine show that both docking species will preferentially bind to the (1 $\bar{1}$ 0)

surface. A Boltzmann distribution law for the binding energies of 2-methylpyrimidylaldehyde predicts the exposure of the pro-*S* face (>90%, albeit, energetically, a weak diastereoselectivity) on the (1 $\bar{1}$ 0) surface. This program of computations can now be applied on any intermediate in the Soai process so as to define the role of crystal surfaces in chirality determination during asymmetric autocatalysis.

Acknowledgments BK thanks the United States National Science Foundation (NSF) for support of this research. ALR and DJC acknowledge the National Computational Infrastructure (NCI) National Facility and iVEC for access to computational resources. We are grateful to John Freudenthal for his efforts to establish the absolute structure of the crystals of γ-glycine optically.

References

1. Avalos M, Babiano R, Cintas P, Jimenez JL, Palacios JC (1997) Tetrahedron 8:2997–3017
2. Soai K, Kawasaki T (2008) Top Curr Chem 284:1–33
3. Soai K, Shibata T, Sato I (2004) Bull Chem Soc Jpn 77:1063–1073
4. Soai K, Shibata T, Sato I (2000) Acc Chem Res 33:382–390
5. Soai K, Shibata T, Morioka H, Choji K (1995) Nature 378:767–768
6. Gehring T, Busch M, Schlageter M, Weingand D (2010) Chirality 22:E173–E182
7. Kawasaki T, Matsumura Y, Tsutsumi T, Suzuki H, Ito M, Soai K (2009) Science 324:492–495
8. Singleton DA, Vo LK (2002) J Am Chem Soc 124:10010–10011
9. Singleton DA, Vo LK (2003) Org Lett 5:4337–4339
10. Islas JR, Lavabre D, Grevy J-M, Lamoneda RH, Cabrera HR, Micheau J-C, Buhse T (2005) Proc Natl Acad Sci 102:13743–13748
11. Siegel JS (1998) Chirality 10:24–27
12. Mislow K (2003) Collect Czech Chem Commun 68:849–864
13. Soai K, Kawasaki T (2006) Chirality 18:469–478
14. Blackmond DG (2010) Cold Spring Harbor Persp Biol 2:a002147
15. Lahav M, Weissbuch I (2011) Chem Rev 111:3226–3267
16. Sato I, Kadowaki K, Soai K (2000) Angew Chem Int Ed 39:1510–1512
17. Soai K, Osanai S, Kadowaki K, Yonekubo S, Shibata T, Sato I (1999) J Am Chem Soc 121:11235–11236
18. Sato I, Kadowaki K, Urabe H, Jung JH, Ono Y, Shinkai S, Soai K (2003) Tetrahedron Lett 44:721–724
19. Kawasaki T, Harada Y, Suzuki K, Tobita T, Florini N, Palyi G, Soai K (2008) Org Lett 10:4085–4088
20. Kawasaki T, Suzuki K, Hatase K, Otsuka M, Koshima H, Soai K (2006) Chem Commun 1869–1871
21. Kawasaki T, Suzuki K, Hakoda Y, Soai K (2008) Angew Chem Int Ed 47:496–499
22. Soai K, Sato I (2002) Chirality 14:548–554
23. Kawasaki T, Jo K, Igarashi H, Sato I, Nagano M, Koshima H, Soai K (2005) Angew Chem Int Ed 44:2774–2777
24. Klankermayer J, Gridnev ID, Brown JM (2007) Chem Commun 30:3151–3153
25. Ercolani G, Schiaffino L (2011) J Org Chem 76:2619–2626
26. Schiaffino L, Ercolani G (2010) Chem Eur J 16:3147–3156
27. Schiaffino L, Ercolani G (2009) Chem Phys Chem 10:2508–2515
28. Bernal JD (1931) Z Kristallogr 78:363–369
29. Iitaka Y (1961) Acta Crystallogr 14:1–10
30. He G, Bhamidi V, Wilson SR, Tan RBH, Kenis PJA, Zukoski CF (2006) Cryst Growth Des 6:1746–1749
31. Rungsimanon T, Yuyama K-I, Sugiyama T, Masuhara H, Tohnai N, Miyata M (2010) J Phys Chem Lett 1:599–603
32. Weissbuch I, Leisorowitz L, Lahav M (1994) Adv Mater 6:952–956
33. Dillip GR, Raghavalah R, Mallikarjuna K, Reddy CM, Bhagavannarayana G, Kumar VR, Raju BDP (2011) Spectrochim Acta Part A Mol Biomol Spectr 79:1123–1127
34. Soai K (2012) private communication
35. Blackmond DG, McMillan CR, Ramdeehul S, Schorm A, Brown JM (2001) J Am Chem Soc 123:10103–10104
36. Buono FG, Blackmond DG (2003) J Am Chem Soc 125:8978–8979
37. Blackmond DG (2004) Proc Natl Acad Sci USA 101:5732–5736
38. Buono FG, Iwamura H, Blackmond DG (2004) Angew Chem Int Ed 43:2099–2103
39. Klussmann M, Iwamura H, Mathew SP, Wells DH, Pandya U, Armstrong A, Blackmond DG (2006) Nature 441:621–623
40. Blackmond DG (2006) Tetrahedron 17:584–589
41. Gridnev ID, Serafimov JM, Quiney H, Brown JM (2003) Org Biomol Chem 1:3811–3819
42. Gridnev ID, Brown JM (2004) Proc Natl Acad Sci USA 101:5727–5731
43. Gridnev ID, Serafimov JM, Brown JM (2004) Angew Chem Int Ed 43:4884–4887
44. Brown MJ, Gridnev I, Klankermayer J (2008) Top Curr Chem 284:35–65
45. Schiaffino L, Ercolani G (2008) Angew Chem Int Ed 47:6832–6835
46. Kahr B, Shtukenberg A, Gunn E, Carter DJ, Rohl AL (2011) Cryst Growth Des 11:2070–2073
47. Accelrys Software Inc (2008) Materials studio release notes, release 4.4. Accelrys Software Inc, San Diego
48. Soler JM, Artacho E, Gale JD, Garcia A, Junquera J, Ordejon P, Sanchez-Portal D (2002) J Phys Condens Matter 14:2745–2779
49. Perdew JP, Burke K, Ernzerhof M (1996) Phys Rev Lett 77:3865–3868
50. Dauber-Osguthorpe P, Roberts VA, Osguthorpe DJ, Wolff J, Genest M, Hagler AT (1988) Proteins Struct Funct Genet 4:31–47
51. Sun H (1988) J Phys Chem B 102:7338–7364
52. Sun H, Ren P, Fried JR (1988) Comp Theor Polym Sci 8:229–246
53. Kvick A, Canning WM, Koetzle TF, Williams GJB (1980) Acta Crystallogr Sect B 36:115–120
54. Desiraju GR, Steiner T (2001) The weak hydrogen bond in structural chemistry and biology. Oxford University Press, Oxford
55. Bijvoet JM, Peerdeman AF, van Bommel AJ (1951) Nature 168:271–272
56. Flack HD, Bernardinelli G (2008) Chirality 20:681–690
57. Dittrich B, Strumpel M, Schafer M, Spackman MA, Koritsanszky T (2006) Acta Crystallogr Sect A 62:217–223
58. Weckert E, Hummer K (1997) Acta Crystallogr Sect A 53:108–143
59. Kaminksy W, Jin L-W, Powell S, Maezawa I, Claborn K, Branham C, Kahr B (2006) Micron 37:324–338
60. Clarborn K, Herreros CJ, Isborn C, Zoulay A, Weckert E, Kaminksy W, Kahr B (2006) J Am Chem Soc 128:14746–14747
61. Weissbuch I, Leiserowitz L, Lahav M (2008) Chirality 20:736–748